2017-04-05

Thermal Characterization of Natural and Synthetic Spider Silks by Both the 3ω and Transient Electrothermal Methods

Troy Munro
Mechanical Engineering Department, Brigham Young University, troy.munro@byu.edu

Changhu Xing
Mechanical and Aerospace Engineering Department, Utah State University

Heng Ban
Department of Mechanical and Aerospace Engineering, Utah State University

Cameron G. Copeland
Synthetic Bioproduct Center, Biology Dept., Utah State University

Randolph V. Lewis
Synthetic Bioproduct Center, Biology Dept., Utah State University

See next page for additional authors

Original Publication Citation

Xing, C., Munro, T., Jensen, C., Ban, H., Copeland, C., and Lewis, R., "Thermal Characterization of Natural and Synthetic Spider Silks by Both the 3ω and Transient Electrothermal Methods," Materials & Design, 119, 2017.

Thermal Characterization of Natural and Synthetic Spider Silks by Both the 3ω and Transient Electrothermal Methods

Changhu Xing[a], Troy Munro[b], Colby Jensen[a], Heng Ban[a]

Cameron G. Copeland[c], Randolph V. Lewis[c]

[a]Department of Mechanical & Aerospace Engineering, Utah State University, Logan, UT 84322

[b]Department of Mechanical Engineering, Brigham Young University, Provo, UT 84602

[c]Synthetic Bioproducts Center, Utah State University, North Logan, UT 84341

Abstract

Thermal conductivity, thermal diffusivity and volumetric heat capacity of three spider silks are measured in this paper as a benchmark for further studies. These silks include the major and minor ampullate silks of the *Nephila clavipes* spider, and a synthetic spider silk fiber made from recombinant dragline silk proteins purified from transgenic goats' milk. Two complementary measurement techniques are employed in the thermal characterization of these microscale single fibers for self-verification. One is the transient electrothermal technique (TET) and the other is the 3ω method. Experimental measurements indicate that thermal properties of the dragline silk are very close to those of the minor ampullate silk, whereas the ones for the synthetic silk are much lower due in part to its low crystallinity. The directly measured thermal conductivity, thermal diffusivity, and volumetric heat capacity of the major and minor ampullate silks are 1.2-1.26 $Wm^{-1}K^{-1}$, 5.7-6 $x10^{-7}$ m^2s^{-1}, and 2-2.17 $MJm^{-3}K^{-1}$, respectively. The thermal conductivity and thermal diffusivity of the as-spun synthetic silk are 0.24 $Wm^{-1}K^{-1}$ and 1.6 $x10^{-7}$ m^2s^{-1} respectively. As part of this study, a detailed comparison of the TET and 3ω methods is provided showing the complementary nature of the techniques and illustrating the strengths and weaknesses of each.

Key words: 3-omega, spider silk, thermal characterization, transient electrothermal technique, synthetic silk

1. Introduction

Naturally spun spider silk has many potential applications such as bullet proof vests, wear-resistance light clothing, ropes or parachutes, or artificial tendons or ligaments due to its favorable mechanical properties [1]. However, it cannot be produced in commercial scale quantities, which has led to the current development of synthetic (artificial) silk fibers by different approaches. The method used in the current study involves transferring silk producing genes to goats, causing the proteins to be expressed in the goats' milk, whereupon the proteins are purified into powders, and are then spun into large quantities of silk fibers with a modified plastic extruder [2]. Although variations in the spinning process (i.e. solvent baths and stretching) give rise to varying mechanical properties, this study focuses on the most basic "as-spun" fiber that experiences no additional processing after the fiber coagulation in isopropanol.

While mechanical properties of the spider silks have been measured with consistent results, thermophysical property measurements are still in the initial stage. Since silk is often touted as a replacement for petroleum-based aramids (such as Kevlar or Nomex), there is a need to also characterize its thermal properties for applications like thermal protective clothing, where aramid fibers are extensively used. For the natural spider silk, there are only two recent reports in the literature with reasonable thermal property values. Using a lock-in infrared thermography technique [3], the thermal diffusivity (α [m^2s^{-1}]) of the *Araneus diadematus* dragline silk was reported as $2x10^{-7}$ m^2s^{-1}. From the transient electrothermal technique (TET) [4], thermal conductivity (k [$Wm^{-1}K^{-1}$]) and thermal diffusivity of the *Nephila clavipes* dragline silk were determined as 1.2 $Wm^{-1}K^{-1}$ and $6x10^{-7}$ m^2s^{-1}, respectively. The measured thermal diffusivity by the authors [4] is within a factor of three to that in Ref. [3]. Therefore, confirmation of the result using another technique is necessary. Furthermore, thermal measurements of other types of silk, or of the synthetic silk fibers, have not been found in literature.

Two techniques (TET and 3ω) have been investigated and successfully validated to determine the thermal conductivity and diffusivity (and the potential to directly measure the volumetric heat capacity, ρC_p [$Jm^{-3}K^{-1}$]) for single fibers by this group [5-8]. The former is based on the transient voltage response after the step input of a

constant direct current (dc), and the latter is analyzed from the steady-state, 3rd harmonic voltage amplitude and phase responses based on a modulated alternating current (ac) heating. In this paper, thermal characterization of individual fibers will adopt one or both of the techniques, depending on the fiber characteristics.

The objective of this paper is to determine the thermal properties of the natural and synthetic fibers. Because of the differences in geometry and properties, a single method cannot measure all of the samples accurately. To this end, technique selection for a specific fiber is provided by comparing the advantages and disadvantages of the two methods based on sample geometry, property, and equipment availability. Thermal properties of the major ampullate, minor ampullate, and synthetic silk fibers are then measured. This paper is crucial for the ongoing synthetic silk production by providing a metric to direct synthetic production to more closely mimic natural spider silk properties.

2. Measurement techniques

Table 1 presents a comparative summary of the TET and 3ω measurement methods. Comparisons are made with respect to measurement theory, procedure, data reduction, and accuracy.

A. Theoretical basis

In order to have a thermal measurement by either of the two methods, the sample needs to have a distinct (uniform) geometry and a large aspect ratio ($L/D > 10$, where L is length [m] and D is diameter [m]). Additionally, it is assumed that in the measured temperature range, the resistivity of the sample changes linearly with temperature, and the temperature coefficient of resistivity (α_T [K^{-1}]) or of resistance (R' [ΩK^{-1}], $R'=R_0\alpha_T$ where R_0 [Ω] is the resistance at temperature T_0 [K]) needs to be known or calibrated. Samples are placed in a high vacuum chamber (<$1x10^{-3}$ - $1x10^{-4}$ Pa)[6] to reduce the lateral heat loss by convection. From the thermal response after heating, the thermophysical properties are then obtained. Both methods use the same sample preparation methods and employ Joule heating as a heat mechanism. The implementation of electrical heating and data detection steps are where the techniques differ.

B. Heat transfer modeling

B.1. TET

To perform the heating in TET, a constant dc current, I_d [A], is needed and can be provided by a precision current source with a negligible settling time. When a constant dc current is applied, the conductive fiber or thin gold film coating heats up. This temperature rise induces a change in resistance, which is monitored by a change in voltage as a function of time. In this way, the sample's response evolves from its initial resistance, R_0, to the steady state value R_s [Ω], corresponding to an average temperature rise, $\Delta T \rightarrow (0, \Delta T_s)$ [K]. Modeling of the heat transfer through the sample has been given in a previous research [5], with the relevant equations for thermal property determination summarized below.

$$k = \frac{4{I_d}^2 R_0 R' L}{\pi D^2 (R_s - R_0)} \frac{2 - 2\cosh(LH_e) + LH_e \sinh(LH_e)}{(LH_e)^3 \sinh(LH_e)} \tag{1}$$

$$\frac{\Delta T}{\Delta T_s} = 1 - \frac{8(LH_e)^3 \sinh(LH_e)}{2 - 2\cosh(LH_e) + LH_e \sinh(LH_e)} \times \sum_{n=1}^{\infty} \frac{e^{-\left[(2n-1)^2\pi^2 + (LH_e)^2\right]\alpha t / L^2}}{\left[(2n-1)\pi\right]^4 + \left[LH_e(2n-1)\pi\right]^2}, \tag{2}$$

where $H_e^2=[(h_r+h_c)A_l-I_d^2R']/(kV_s)$ represents the heat loss from the radial surface and variable heating due to the resistance change. The parameter h_r is the linearized radiation coefficient ($h_r \approx 4\varepsilon\sigma T_0^3$, where ε is emissivity and σ is the Stefan-Boltzmann constant); h_c is the convective heat transfer coefficient [$Wm^{-2}K^{-1}$]; and A_l and V_s are the lateral

surface area [m^2] and sample volume [m^3], respectively. These additional terms are necessary for correct representation of the relevant heat transfer mechanisms and accurate property determination.

The temperature rise is usually limited to 2-10 K[4, 9], to minimize the heat generation drift (I_d^2R') induced by the resistance change. However, for the coated, non-conductive samples, a low temperature rise causes relatively large error in the property measurements because of a low signal-to-noise ratio. Therefore, an optimal current is generally sought in the measurement to balance these two concerns. With negligible variation of heating and the high vacuum to minimize convection ($h_c \approx 0$), the only term in H_e requiring special consideration is the radiation heat loss. This heat loss is independent of the temperature rise but not of the sample length. This will be discussed in the data reduction section.

To detect the transient response (Fig. 4 in Ref. [9]), a data acquisition unit/digital multimeter (DMM) with a fast sampling rate and high accuracy is needed. Depending on the sample length and thermal diffusivity, the sampling time varies from milliseconds to several hundred seconds.

B.2 3ω

In the 3ω measurement, a modulated ac current, with an amplitude of I_0 [A] and frequency of ω [rad/s], is passed through the sample to generate electrical heating at the 2ω frequency. This induces a temperature response at 2ω (negligible for higher harmonics), and then a 2ω response in the electrical resistance (Tab. 1). The voltage response then has harmonics at odd ω. Detection of the voltage change is performed on the 3ω response ($I_0R'\cos\omega t \bullet \Delta T(2\omega t)$) because it has the best accuracy. Modeling of the heat transfer by the 3ω method for thin fibers has been performed previously [7]. The detected voltage in a complex form is expressed by Eq. 3.

$$V_3 = \frac{I_0^3 R_0 R' L}{k\pi D^2} \frac{2 - 2\cosh(Lm) + Lm\sinh(Lm)}{L^3 m^3 \sinh(Lm)}, \quad (3)$$

where $m^2=i2\omega/\alpha+4h_r/(Dk)$ represents the heating frequency and radiation influences on the measured voltage amplitude and phase responses. With negligible convective heat loss and nonconstant heating influences in both TET & 3ω measurements, $m^2=i2\omega/\alpha+H_e^2$.

To experimentally detect the voltage response from Eq. 3, a lock-in amplifier is usually employed to monitor the 3rd harmonic frequency. With a continuous ac source heating the sample, the voltage amplitude and phase (φ) are measured once they reach their steady state values. Usually, a frequency range that allows the phase to go between (0, -90°) is scanned to get the amplitude- or phase-frequency curve (Fig. 3 in Ref. [7]) used for the inverse problem of extracting thermal properties. Note that the voltage measured by a lock-in amplifier is a root-mean-square (rms) value.

C. Thermophysical property extraction process

Comparing Eq. 1 with Eq. 3 indicates that the radiation influence in the TET and 3ω technique (m or H_e terms) are the same, seen as $4h_r/(Dk)$. To account for radiation heat loss when ε is unknown, a model with dependency on one thermal property is used to calculate that property and ε. Then the other property is determined with the now calculated ε value.

For the TET, thermal conductivity and diffusivity are obtained from Eq. 1 and 2. However, since the radiation influence cannot be avoided, multiple length samples are necessary to separate the radiation contribution from the measured thermal properties. One approach ($k, \varepsilon \rightarrow \alpha$) uses Eq. 1 to determine k and ε. Eq. 2 is then used to obtain α. For samples with large uncertainty from measured R', this procedure renders large error. For such samples, the suggested process ($\alpha, H_e \rightarrow k$) is to start from Eq. 2 to determine α and H_e. With H_e, the k of each sample can then be determined by Eq. 1. The latter procedure is preferred because of lower precision uncertainties in measured thermal diffusivity [9] than thermal conductivity.

For the 3ω method, thermal conductivity, diffusivity, and volumetric heat capacity (which is equal to the product of density ρ [kgm^{-3}] and specific heat capacity C_p [$Jkg^{-1}K^{-1}$]) can be determined independently from Eq. 3 at different frequency ranges. At frequencies where $\varphi < -5°$ (i.e. low-frequency range), the amplitude from Eq. 3 becomes

independent of frequency and dependent only on thermal conductivity (and radiation heat loss). Similar to the TET, k can be obtained by curve-fitting based on property measurements of samples at different lengths or by knowing H_e.

Within the frequency range where $-90° < \varphi < -89°$ (i.e. high-frequency range), the amplitude from Eq. 3 depends on the product of ρC_p only. Radiation has little effect on the amplitude response in this frequency range, which is an advantage of the direct measurement of ρC_p. However, the signal becomes much weaker and susceptible to system noise. To measure an equivalent amplitude response similar to that seen at low frequencies, the temperature rise has to become large, which may violate the constant heating assumption. However, even with these uncertainties, the direct determination of ρC_p is still one of the benefits of the 3ω measurement.

In the middle frequency range, the phase-frequency response is used for thermal diffusivity evaluation by direct fitting of Eq. 3. The regression is similar to the second procedure for TET (α, $H_e \rightarrow k$) but is easier because fewer data points are typically measured in the 3ω method.

D. Selection considerations for both techniques

Properties Determined: The 3ω technique allows three properties (k, α, ρC_p) to be measured simultaneously and independently. This prevents the propagation of uncertainty from two parameters when calculating the third ($\rho C_p = k/\alpha$). From the TET, however, only k and α are available for simultaneous determination.

Accuracy: The 3ω technique has better accuracy than the TET. The amplitude of 3ω measurements is a function of only sample resistance, R_0, whereas for the TET, thermal conductivity is derived from the temperature rise resulting in the change of sample resistance, R_s-R_0. The resistance change in the measurement is only several thousandths or ten-thousandths of the sample resistance, producing larger precision uncertainties in the TET. Uncertainties associated with the correct selection of the initial unheated resistance from the transient curve and good acquisition of the transient nature of the heating effect [9] further decrease the accuracy of the TET approach. The 3ω measures the signal in a steady-state manner, which improves the accuracy of the phase and amplitude by averaging the signal over a period of time.

Measurement Time: The advantage of the TET over the 3ω method is in measurement time, from millseconds to hundreds of seconds depending on the sample length and diffusivity. In comparison, the 3ω method typically require minutes to hours to reach steady-state conditions at a single frequency. For high diffusivity samples, 3ω is the preferred choice due to the better accuracy. For low diffusivity samples, if the diameter is sufficiently small such that the radiation influence is significant (e.g. natural spider silks), the 3ω technique is favorable. But if the diameter is large and the samples are long (e.g. synthetic spider silk), the TET has advantages due to the prohibitively long measurement time of the 3ω method (at frequencies <0.01 Hz).

Radiation Influence: Both methods suffer from the radiation heat loss influence, therefore, it is infeasible to get the precise property measurement with one sample. Tests at various lengths need to be performed before to ensure proper accounting of radiation heat transfer effects.

3. Samples and tests

A. Silks

Thermal properties of dragline (major) silk of the *Nephila clavipes* have yet to be measured and verified by the 3ω method, but have been investigated using the TET in a previous research [4]. This major ampullate silk is comprised of two proteins, MaSp1 and MaSp2. In this paper, data reduction on the TET measurements will be conducted based on direct diffusivity measurements (α, $H_e \rightarrow k$ in Sec. 2C), and compared with results from the direct measurements of the conductivity (k, $\varepsilon \rightarrow \alpha$) [4]. In the 3ω measurement, one fiber was broken from set (a sample set is defined in Sec. 3B) #2, thus leaving 12 samples of the original 13 from Ref [4]. However, the broken fiber was not replaced because there would have been a need for additional coating and annealing, but the broken fiber did not cause any problems to the silk measurements. The diameter of the major silk was 3.1±0.2 μm, measured by a scanning electron microscope (SEM). The silks on each sample mount set are taken from the same strand of spider silk.

Minor ampullate silk is produced from the minor ampullate gland of the spider and is comprised of MiSp1 and MiSp2 proteins. These proteins have similar secondary structures to the major ampullate or dragline silk, but not all

structures are present, nor are all mechanical properties the same. The primary structures of the two silks are distinctly different [10], and the extensibility and tensile strength are different. Additionally, minor ampullate contains complex spacers that are not in major ampullate silk [11], while major ampullate silk has GPGXX motiffs which are responsible for the extensibility of the silk. The diameter of the minor ampullate silk was 2±0.2 μm under SEM measurement. Three sets of samples have been prepared and measured by both techniques for comparison.

Both major and minor ampullate silk was collected from adult *N. clavipes* spiders, which originated from Florida, US, using the method described by Xu et al. [12] (similar to Ref. [13]). Briefly, spiders were restrained on the top of a Petri dish and anesthetized by exposing them to CO_2.The spider's spinnerets were located with a dissecting microscope and using tweezers, whereupon the silk was teased out of either the major or minor ampullate gland. The silk was attached to a rotating spool and was gathered continuously at a silking rate of about 2 m/min. During the spooling procedure, the spiders were misted with water. Samples placed on the heat sinks of each measurement set were unwound from these spools so that all samples on all the sets came from the same strand of silk.

The protocol for synthetic silk gene cloning, protein expression, protein purification, and fiber formation is detailed in Refs. [14-16], and a summary of the relevant processes is given. The dragline proteins, MaSp1 and MaSp2, were expressed in the milk of different goat herds. The protein was then extracted and purified from the milk, resulting in a white powder. For the current study, a ratio of 80% MaSp2 to 20% MaSp1 by weight for the proteins was dissolved in Hexafluoro-2-propanol (HFIP) to create a dope (about 20% weight/volume (w/v) concentration of protein in the dopes). The dope was then pushed out of a small diameter syringe (254 μm) into a 100% isopropanol bath, which caused the dope to coagulate. The coagulated, extruded silk was then fed through godets and collected on a winder. These "as spun-fibers" (no additional treatment, except for the coagulation bath) were selected for thermal property characterization because of their uniform geometry, in addition to providing a benchmark property. Under SEM, the diameter was 51.7±1 μm. Because of its large diameter (less radiation influence) and low expected thermal conductivity, the synthetic fiber was mainly measured by TET. For the shortest synthetic fiber, which required a modulation frequency near 0.005 Hz to get thermal conductivity, the 3ω technique is used to verify the TET measurements.

SEM pictures of the three types of fibers are presented in Fig. 1.

B. Sample preparation and equipment

Preparation of the electrically non-conductive samples for both TET and 3ω has been detailed elsewhere [9]. Briefly, one end of a sample is mounted on a common heat sink and the other was separately secured on a different heat sink terminal. This process was repeated several times until silks from the same strand were placed on a sample mount set. Because the silks were from the same strand, there was little difference between the behavior of each set. The set of samples underwent gold sputter coating, annealing, and its temperature coefficient of resistivity was calibrated in an isothermal enclosure. The two measurement techniques were then employed with the samples placed in a high vacuum chamber. The number of samples on a mount is limited by the size of the gold sputter coater thus a maximum of 8 samples were prepared in a set. However, because of coating defects, not all samples exhibited a measurable resistance and could therefore be measured. Because the thermal property measurement of the dragline silk by TET [4] revealed lower thermal properties than originally expected, the minor ampullate silk sample sets were prepared with shorter sample lengths to reduce measurement times.

Water content in silk has the effect of increasing the storage modulus of the fiber when the water is removed [17], which results in a glassy rather than rubbery state of the silk [18]. With regard to the loss of water by the silk during the coating process and property measurement, the silk is expected to have a slightly higher property than if the fibers were in a state of supercontraction due to a high relative humidity. All other thermal property measurements of silk in the literature have also employed high vacuum.

For the TET measurement, a Keithley 6221 current source with a short settling time was selected for the constant dc heating. A Keithley 3706 DMM was employed to monitor the voltage change in a four wire resistance measurement configuration. For the 3ω measurement, an SR 850 lock-in amplifier was employed to both provide a constant ac voltage and monitor the 3rd harmonic voltage response (complex number). The sample was connected to a custom Wheatstone bridge, and conversion of the constant voltage output to constant current models can be found in Ref. [7]. In the 3ω measurement, a Keithley 6221 in ac mode was also employed for some samples as a comparison.

Thermal properties of the fibers were determined by the equations in Sec. 2B and methods in Sec. 2C.

4. Results and discussion

The thermophysical properties of the three silk samples (dragline, minor ampullate, and synthetic) are discussed in this section. Figures showing the variation with respect to length will be presented to demonstrate how the full model corrects for radiative heat losses to improve measurement accuracy.

Dragline Silk TET:

Figure 2 presents the thermal diffusivity and thermal conductivity of the dragline silk measured by the TET (α =5.9x10^{-7} m^{2}s^{-1}, k=1.18 Wm^{-1}K^{-1}). Data reduction for property extraction employs the second approach in Sec. 2C (α, $H_e \rightarrow k$), namely getting α and H_e from Eq. 2 by regression on 13 sample measurements. Then k can be obtained from Eq. 1 by the knowledge of H_e. A least-squares regression method is used to obtain k or α. Because radiation heat loss significantly influences the measured thermal property, the measured thermal conductivity (neglecting heat loss) varies from 1.2 to ~200 Wm^{-1}K^{-1}, depending on the sample length (Tab. 1 in Ref. [4]). The determined thermal conductivity and diffusivity by the second approach (α, $H_e \rightarrow k$) compared with those obtained using the first approach (k, $\varepsilon \rightarrow \alpha$ in Ref. [4]) show small differences. The comparison provides evidence of reliable measurement for both the thermal conductivity and diffusivity since it is not model dependent. Separate regressions using Eq. 1 or 2 uncouple k and α, and are thus not recommended in the characterization. Consistency of the results provide greater confidence that the results are independent of the data processing approach and related only to the thermal behavior of the samples.

Dragline Silk 3ω:

Figure 3 presents a dragline silk measurement by the 3ω technique. When φ>-5°, the amplitude response stays almost constant and depends only on sample k and LH_e (H_e is the unknown and LH_e is dimensionless whereas m has frequency contribution). With the assumption that $LH_e \rightarrow 0$, k can be determined directly, with the results presented in Tab. 2 as the R (reduced) column. Similar to Fig. 3, k of other silks at multiple lengths is also determined and presented in Tab. 2. As can be seen from the table, the calculated k varies in two orders of magnitude, which indicates a significant heat loss effect, and thus, the need for the full Eq. 3.. With the least-squares minimization, a regressed k and H_e can be obtained and the individual k of each sample is presented in Tab. 2 as the F (full) column.

In the middle frequency range of Fig. 3, the phase response is used for the α determination of the dragline silk. Using the previously calculated H_e, the determined α with and without included heat loss effects is presented in Tab. 2. As observed in the earlier k determination, significant heat loss contribution is found as the length of the fiber increases. At the high frequency range (which also corresponds to when $\varphi \rightarrow$-90°), the amplitude is employed to determine ρC_p. The directly measured ρC_p given in the table is comparable to the value calculated by k/α.

Figure 4 summarizes the measured k, α, and ρC_p of dragline silk in Tab. 2 and further presents the properties determined from the approach of $\alpha \rightarrow k$ (Fig. 4b). As can be seen from Fig. 4a and 4b, the results are almost identical. The directly measured ρC_p (Fig. 4c) is used to verify the accuracy of the former two properties (k and α). As shown in the figure, the directly measured ρC_p is only 2% different from that computed from k/α. In addition, measurements by the 3ω technique confirm the results presented in Ref. [4]. The scatterings (two standard deviations about the mean of the measurements) are respectively 15%, 12%, and 15% for α, k, and ρC_p measurements.

Minor Ampullate Silk TET and 3ω:

The minor ampullate silk has been measured by the two techniques, and the results are presented in Fig. 5 and Tab. 3. For both, the thermal diffusivity is determined, with H_e determination being the first step in the data processing (α, $H_e \rightarrow k$). As shown in Fig. 5b, several outliers are neglected from the k and ρC_p dataset based on Chauvenet's criterion. These outliers are likely ascribed to diameter uncertainty, the calibration of R', or coating defects for that particular sample. Calibration of R' was conducted several times but none of the calibrations yielded a reasonable k value. However, these defects do not affect the accuracy of α, because thermal diffusivity determination employs a dimensionless transient curve for TET and non-dimensional phase response for 3ω. In the data reduction process, all of the samples are incorporated in the α-regression process and, by using the full models, length considerations were taken into account. Measured properties of minor ampullate silk (α =5.7x10^{-7} m^{2}s^{-1}, k=1.26 Wm^{-1}K^{-1}, and ρC_p = 2.17

$MJm^{-3}K^{-1}$) are close to those of the major silk, with measurement scatterings of 12%, 19%, and 20% for α, k, and ρC_p, respectively. These values do not vary significantly from the major ampullate silk, although their mechanical properties such as extensibility and tensile strength do. The explanation for this is the independence of thermal conductivity on those properties, but by way of a well-known kinetics model for the thermal conductivity of a material ($k=1/3\ \rho C_p \upsilon \Lambda = C_p \Lambda (E\rho)^{-0.5}$, where υ is the speed of the heat carrier [ms^{-1}] – which are phonons in the case of silk, Λ is the mean free path of the heat carrier [m], and E is the Young's Modulus [GPa]), the key properties for thermal conductivity, k, are specific heat and Young's modulus. The work of Koski [19] has shown that the elastic moduli of major and minor ampullate silks from the *N. clavipes* spider is not significantly different. Since these values do not contribute to ultimate tensile strength of extensibility of the silk, having similar thermal properties but different mechanical properties is reasonable.

Synthetic Silk TET and 3ω:

The synthetic silk's thermal properties are presented in Fig. 6 and Table 4. This fiber is mainly measured by the TET, because the H_e term is much smaller due to its relatively large diameter. To verify the TET measurements, the 3ω technique is also used for the shortest sample. Diffusivity and conductivity of the synthetic fiber are 1.6×10^{-7} m^2s^{-1} and 0.24 $Wm^{-1}K^{-1}$, respectively. Using the measured thermal conductivity and diffusivity, the volumetric heat capacity may be calculated as 1.5 $MJm^{-3}K^{-1}$, ~25% lower than the natural spider silk. For the synthetic fiber measurements, the scatterings are 15% and 13% for α and k measurements, respectively.

Thermal conductivity and diffusivity of the synthetic fiber is much smaller than the natural silk, which agrees with its low degree of crystallinity and lower mechanical properties (particularly Young's Modulus) compared to the dragline silk [20, 21]. For conditions that require thermal insulation, the synthetic fiber is more suitable; for conditions that necessitate larger thermal conductivity, other treatments on the as-spun fiber (that increase the crystallinity and mechanical properties of the fiber [2]) may be able to improve the thermal properties. This improvement comes from the formation and axial alignment of crystalline β-sheets that are expected to have a higher thermal conductivity than the amorphous regions of the fiber [22]. Such treatments are under investigation but currently produce a fiber with a non-uniform geometry [23, 24], which creates large uncertainty on the measured property values.

It should be noted that the influence of the metallic coating on the measured thermal properties has been investigated previously [9], but the change of measured property values due to an increase of coating thickness (10 nm to 20 nm) is within the uncertainty range of measurements (±5%) [9]. The relative roughness of the synthetic silk is not expected to double the coating thickness size, nor affect the property measurement within the current uncertainty bounds. The uncertainty caused by the coating is primarily related to nonuniformity in the coating and the fact that the metallic film (10nm) behaves differently (non-constant resistivity and significant thermal conductivity drop) from the bulk material, even after annealing [4, 9].

5. Conclusions

To aid in the selection of an appropriate technique for the thermophysical property measurements of different spider silks (or thin fibers), the advantages and disadvantages of the TET and steady-state 3ω method are compared with respect to measurement theory, data processing, and measurement accuracy. The 3ω technique generally has a better measurement precision and is preferred, if feasible. For samples that would experience a prohibitively long measurement time with the 3ω method, the TET is a reliable alternative.

Data processing where the thermal diffusivity and radiation influence is determined first and the conductivity determination is done based on those results (α, $H_e \rightarrow k$) is preferred because only dimensionless data are required. Coating anomalies or other defects that significantly affect the thermal conductivity or heat capacity measurements have little influence on the accuracy of thermal diffusivity evaluation relative to other measurement uncertainties.

Experimental measurements indicate that the minor ampullate silk has equivalent thermal properties to the major silk. The thermal conductivity and diffusivity of the untreated, as-spun synthetic silk fiber are respectively ~1/5 and ~1/4 of the properties of the natural dragline spider silk, primarily attributed to its low degree of crystallinity. The results also demonstrate the use of these techniques as a powerful tool for providing comparative metrics directly linked to material microstructure. Such metrics will aid development of synthetic production of spider silk to more closely mimic natural spider silk properties.

Acknowledgments

Partial support by Utah Science Technology and Research (USTAR) initiative funding. The gold coating and SEM work were performed by FenAnn Shen at the Nanoscale Device Laboratory, USU.

References

[1] R.V. Lewis, Spider Silk: Ancient Ideas for New Biomaterials, Chem. Rev. 106 (2006) 3762-3774.
[2] C.G. Copeland, B.E. Bell, C.D. Christensen, R.V. Lewis, Development of a Process for the Spinning of Synthetic Spider Silk, ACS Biomater. Sci. Eng. 1(7) (2015) 577-584.
[3] R. Fuente, A. Mendioroz, A. Salazar, Revising the Exceptionally High Thermal Diffusivity of Spider Silk, Mater. Lett. 114 (2014) 1-3.
[4] C. Xing, T. Munro, B. White, H. Ban, C. Copeland, R. Lewis, Thermophysical Properties of the Dragline Silk of Nephila clavipes Spider, Polymer 55(16) (2014) 4226-4231.
[5] C. Xing, T. Munro, C. Jensen, H. Ban, Analysis of the Electrothermal Technique for Thermal Property Characterization of Thin Fibers, Meas. Sci. Technol. 24(10) (2013) 105603.
[6] C. Xing, T. Munro, C. Jensen, B. White, H. Ban, Thermal Characterization of Fine Fibers using an Improved Direct Electrical Heating Method, Int. J. Thermophys. 35(8) (2014) 1512-1525.
[7] C. Xing, C. Jensen, T. Munro, B. White, H. Ban, M. Chirtoc, Thermal Property Characterization of Fine Fibers by the 3-omega Technique, Appl. Therm. Eng. 71(1) (2014) 589-595.
[8] C. Xing, C. Jensen, T. Munro, B. White, H. Ban, M. Chirtoc, Accurate Thermal Property Measurement of Fine Fibers by the 3-omega Technique, Appl. Therm. Eng. 73 (2014) 315-322.
[9] C. Xing, T. Munro, C. Jensen, B. White, H. Ban, C. Copeland, R. Lewis, Thermophysical Property Measurement of Electrically Nonconductive Fibers by the Electrothermal Technique, Meas. Sci. Technol. 25(11) (2014) 115604.
[10] P. Papadopoulos, R. Ene, I. Weidner, F. Kremer, Similarities in the Structural Organization of Major and Minor Ampullate Spider Silk, Macromol. Rapid Commun. 30(9-10) (2009) 851-857.
[11] C. Fu, Z. Shao, V. Fritz, Animal Silks: Their Structures, Properties and Artificial Production, Chem. Commun. 43 (2009) 6515-6529.
[12] M. Xu, R.V. Lewis, Structure of a Protein Superfiber: Spider Dragline Silk, Proc. Natl. Acad. Sci. 87 (1990) 7120-7124.
[13] R.W. Work, P.D. Emerson, An Apparatus and Technique for the Forcible Silking of Spiders, J. Arachnol. 10 (1982) 1-10.
[14] H.B. Steinkraus, H. Rothfuss, J.A. Jones, E. Dissen, E. Shefferly, R.V. Lewis, The Absence of Detectable Fetal Microchimerism in Nontransgenic Goats (Capra Aegagrus Hircus) Bearing Transgenic Offspring, J. Anim. Sci. 90(2) (2012) 481-488.
[15] F. Teulé, A.R. Cooper, W.A.B. Furin, D. , E.L. Rech, A. Brooks, R.V. Lewis, A Protocol for the Production of Recombinant Spider Silk-Like Proteins for Artificial Fiber Spinning, Nat. Protoc. 4(3) (2009) 341-355.
[16] C.L. Tucker, J.A. Jones, H.N. Bringhurst, C.G. Copeland, J.B. Addison, W.S. Weber, Q. Mou, J.L. Yarger, R.V. Lewis, Mechanical and Physical Properties of Recombinant Spider Silk Films Using Organic and Aqueous Solvents, Biomacromolecules 15(8) (2014) 3158-3170.
[17] J. Guan, D. Porter, F. Vollrath, Thermally Induced Changes in Dynamic Mechanical Properties of Native Silks, Biomacromolecules 14(3) (2013) 930-937.
[18] M. Elices, G.R. Plaza, J. Pérez-Rigueiro, G.V. Guinea, The Hidden Link between Supercontraction and Mechanical Behavior of Spider Silks, J. Mech. Behav. Biomed. 4(5) (2011) 658-669.
[19] K.J. Koski, P. Akhenblit, K. Mckiernan, J.L. Yarger, Non-Invasive Determination of the Complete Elastic Moduli of Spider Silks, Nat. Mater. 12(3) (2013) 262-267.
[20] A.E. Albertson, F. Teulé, W. Weber, J.L. Yarger, R.V. Lewis, Effects of Different Post-Spin Stretching Conditions on the Mechanical Properties of Synthetic Spider Silk Fibers, J. Mech. Behav. Biomed. Mater. 29 (2014) 225-234.
[21] F. Teulé, B. Addison, A.R. Cooper, J. Ayon, R.W. Henning, C.J. Benmore, G.P. Holland, J.L. Yarger, R.V. Lewis, Combining Flagelliform and Dragline Spider Silk Motifs to Produce Tunable Synthetic Biopolymer Fibers, Biopolymers 97(6) (2012) 418-431.

[22] L. Zhang, T. Chen, H. Ban, L. Liu, Hydrogen Bonding-Assisted Thermal Conduction in β-sheet Crystals of Spider Silk Protein Nanoscale 6 (2014) 7786-7791.
[23] G.M. Menezes, F. Teulé, R.V. Lewis, L.P. Silva, E.L. Rech, Nanoscale Investigations of Synthetic Spider Silk Fibers Modified by Physical and Chemical Processes, Polym. J. 45 (2013) 997-1006.
[24] S.L. Adrianos, F. Teulé, M.B. Hinman, J.A. Jones, W.S. Weber, J.L. Yarger, R.V. Lewis, Nephila Clavipes Flagelliform Silk-Like GGX Motifs Contribute to Extensibility and Spacer Motifs Contribute to Strength in Synthetic Spider Silk Fibers, Biomacromolecules 14(6) (2013) 1751-1760.

Table 1 Comparison between the TET and 3ω method

	3ω	TET
Requirement for method applicability	Known or calibrated constant temperature coefficient of resistivity (α_T) such that $R(T)=R_0(T_0)[1+\alpha_T(T-T_0)]$	Same
Sample preparation	Suspended conductive wire or metal-coated non-conductive fiber on heat sinks with well-defined geometry (L, D)	Same
Testing conditions	High vacuum (< ~0.001Pa) to minimize convective heat transfer	Same
Measurement theory	Modulated Joule heating	Transient Joule heating
Heating type	ac current modulated at 1ω	Constant dc current
Heating magnitude (ΔT)	~1/5 of the required heating magnitude by TET	Higher to improve signal strength (unfortunately also induces larger temperature rise, 2-10K)
Detection type	Steady-state voltage amplitude and phase at 3ω of heating frequency via lock-in amplifier	Fast DMM detection during transient temperature increase to reach steady-state
Detection accuracy	High for the fundamental harmonic signal is cancelled	Less, because of the uncertainty in Joule heating initiation, and negligible resistance change compared to the bulk sample resistance (signal-to-noise-ratio)
Thermal conductivity (k)	From low frequency voltage amplitude, proportional to sample resistance, high accuracy	From steady-state temperature rise, proportional to sample resistance change by temperature rise, medium accuracy
Volumetric heat capacity (ρC_p)	From high frequency voltage amplitude, susceptible to noise, medium accuracy	Unable to determine directly
Thermal diffusivity (α)	Regression based on phase at different frequencies, high accuracy	Regression on the transient temperature rise curve, medium to high accuracy
Radiation influence (h_r)	Same influence but the correction is easier to perform based on thermal conductivity (amplitude) or thermal diffusivity (phase)	Length independency needs to be checked for the same samples with same treatments. Correction is necessary at significant levels of influence.
Variable heating influence (I_d^2R' or I_0^2R')	Not necessary because of less heating	Necessary, if larger temperature rise is required for better precision
Measurement length of time	Long (minutes)	Quick (seconds)
Equipment	Lock-in amplifier and either modulated current supply or bridge circuit for voltage supply	DMM and constant current supply

Table 2 Measurement of *dragline silk* by the 3ω technique. Fiber diameter D: 3.1μm; V_3: rms voltage measured by lock-in amplifier when φ >-5°. It was observed that resistances have a slight change after TET measurements. (R: reduced model of Eq. 3 which neglects heat loss $(h_r=0)$ and F: full Eq. 3)

Set #	L (mm)	R_0 (Ω)	R' (ΩK^{-1})	I_0 (μA)	V_3 (μV)	k (Wm^{-1}K^{-1})		α (mm^{2}s^{-1})		ρC_p (MJm^{-3}K^{-1})
						R	F	R	F	
1	3.84	6134.5	5.82	5.5	4.61	9.65	1.35	4.09	0.54	2.29
2	4.53	4914.2	4.76	7.41	7.52	11.18	1.18	5.83	0.57	2.05
2	7.86	7469.1	7	6.81	8.16	31.07	1.21	16.91	0.59	1.96
2	12.31	15306.7	11.24	5.08	7.42	72.86	1.22	42.96	0.62	1.9
3	0.32	792.2	0.63	25	3.95	1.24	1.19	0.58	0.56	2.14
3	1.47	2221.8	2.19	8.5	3.86	2.23	1.15	1.22	0.62	2.02
3	8.83	8939.9	10.33	4.5	3.56	40.74	1.28	21.21	0.59	1.99
3	13.97	16307.4	18	3.5	3.53	97.21	1.27	51.94	0.58	1.86
3	20.24	31436.5	32.08	3.13	6.54	186.36	1.19	118.13	0.64	1.87
4	1.08	1827.1	1.86	13	7.62	2.06	1.37	1.04	0.68	1.95
4	6.46	12435	10.62	4	4.54	23.45	1.31	12.19	0.62	2.26
4	11.62	37611.5	27.05	2.5	5.57	64.68	1.2	41.27	0.67	1.79
Mean							1.24		0.61	

Table 3 Measurement of minor ampullate silk by the 3ω technique. Fiber diameter D: 2 μm; V_3: rms voltage measured by lock-in amplifier when φ >-5°. (R: reduced model of Eq. 3 which neglects heat loss (h_r=0) and F: full Eq. 3). Outliers (grey color) are included in the reduced model & ρC_p measurement, which demonstrates the merit of regression based on thermal diffusivity.

Set #	L (mm)	R_0 (Ω)	R' (ΩK^{-1})	rms I_0 (μA)	V_3 (μV)	k (Wm^{-1}K^{-1})		α (mm^{2}s^{-1})		ρC_p (MJm^{-3}K^{-1})
						R	F	R	F	
1	0.59	726	0.56	21.8	8.4	3.87		0.75	0.59	5.64
1	1.26	2965	1.9	5.77	7.09	2.55	1.18	1.3	0.59	2.11
1	2.46	4220	2.67	5.76	7.94	8.83		2.92	0.52	3.25
1	3.7	5152	5.17	4.28	6.72	15.2	1.44	6.89	0.6	2.46
1	5.14	9520	8.34	3.34	7.9	25.5	1.33	11.8	0.55	2.45
2	0.44	1653	1.25	16.4	7.89	6.81		0.69	0.6	10.7
2	0.91	2523	1.78	8.29	8.31	3.73		0.85	0.52	4.86
2	2.97	4512	4.1	4.97	9.7	9.24	1.27	4.75	0.61	2.03
2	4.23	9824	8.69	3.1	7.8	18.2	1.36	8.71	0.59	2.32
3	0.34	1530	0.93	14.6	9.28	2.16		0.59	0.54	4.01
3	3.48	4755	4.97	4.29	7.24	11.87	1.25	6.14	0.6	2.14
3	7.41	9116	9.14	3.32	7.2	41.6	1.1	23.3	0.54	1.96
3	8.4	21480	18.64	2.16	8.27	54	1.13	29.9	0.54	1.91
Mean							1.26		0.57	2.17

Table 4 Measurement of *synthetic silk* by the TET (R: reduced model of Eq. 3 which neglects heat loss *(h_r=0)* and F: full Eq. 3). Fiber diameter *D*: 51.7μm

Fiber #	*L* (mm)	R_0 (Ω)	*R*' (ΩK^{-1})	*k* (Wm^{-1}K^{-1})		*α* (mm^{2}s^{-1})		ρC_p (MJm^{-3}K^{-1})
				R	F	R	F	
1	1.72	681.2	0.443	0.34	0.25	0.22	0.16	
1 (3ω)	1.72			0.34		0.22		
2	3.69	1169.8	0.786	0.63	0.24	0.46	0.17	
3	6.12	1029.4	0.719	1.12	0.22	0.93	0.16	
4	8.83	1178.4	0.858	2.29	0.24	1.56	0.15	
5	11.02	1676.8	1.206	3.44	0.24	2.30	0.15	
6	12.12	2335.2	1.589	3.98	0.24	3.16	0.17	
7	13.83	5205.0	3.332	5.74	0.27	4.35	0.18	
Mean					0.25		0.16	1.5

Figures

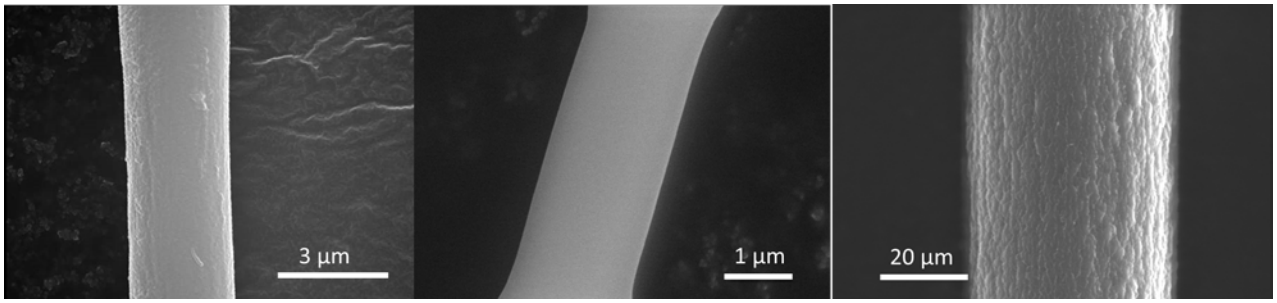

Fig. 1 SEM images of natural dragline silk (left, 3µm scale bar), minor ampullate silk (center, 1µm scale bar), and as-spun synthetic silk (left, 20µm scale bar).

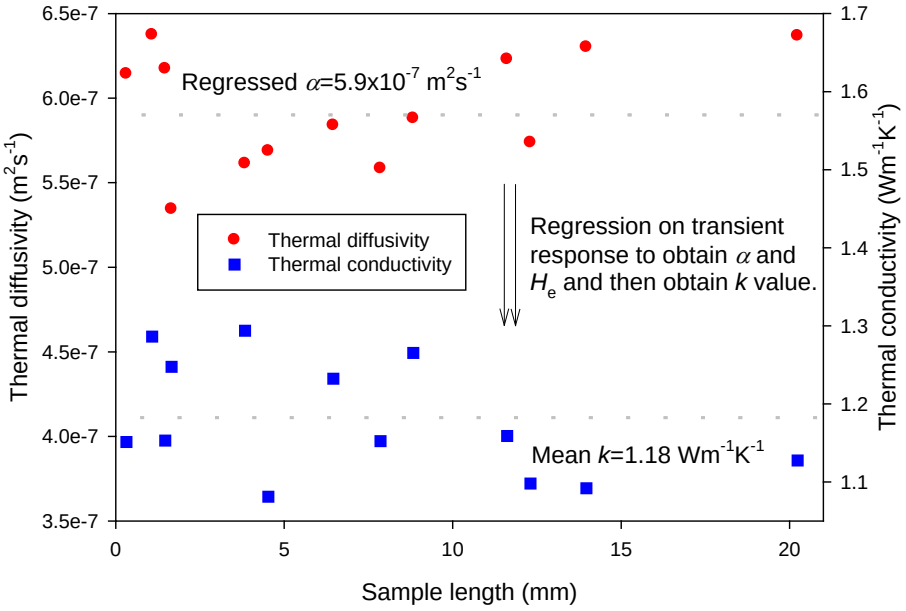

Fig. 2 Thermal properties of *dragline spider silk* measured by the TET. Thermal diffusivity and radiation contribution were determined first and then thermal conductivity (α, $H_e \rightarrow k$) was obtained by incorporating the found radiation influence. Similar results are found using conductivity models first and then diffusivity models (k, $\varepsilon \rightarrow \alpha$).

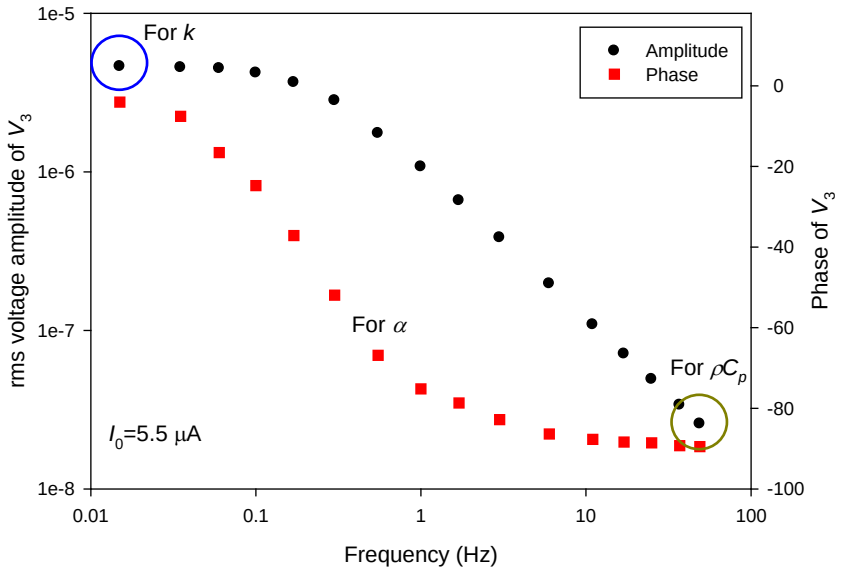

Fig. 3 3ω measurements of one *dragline silk* sample, L=3.84 mm, demonstrating the measured amplitude and phase behavior as a function of frequency, as well as regions of the data used for determination of the different thermophysical properties.

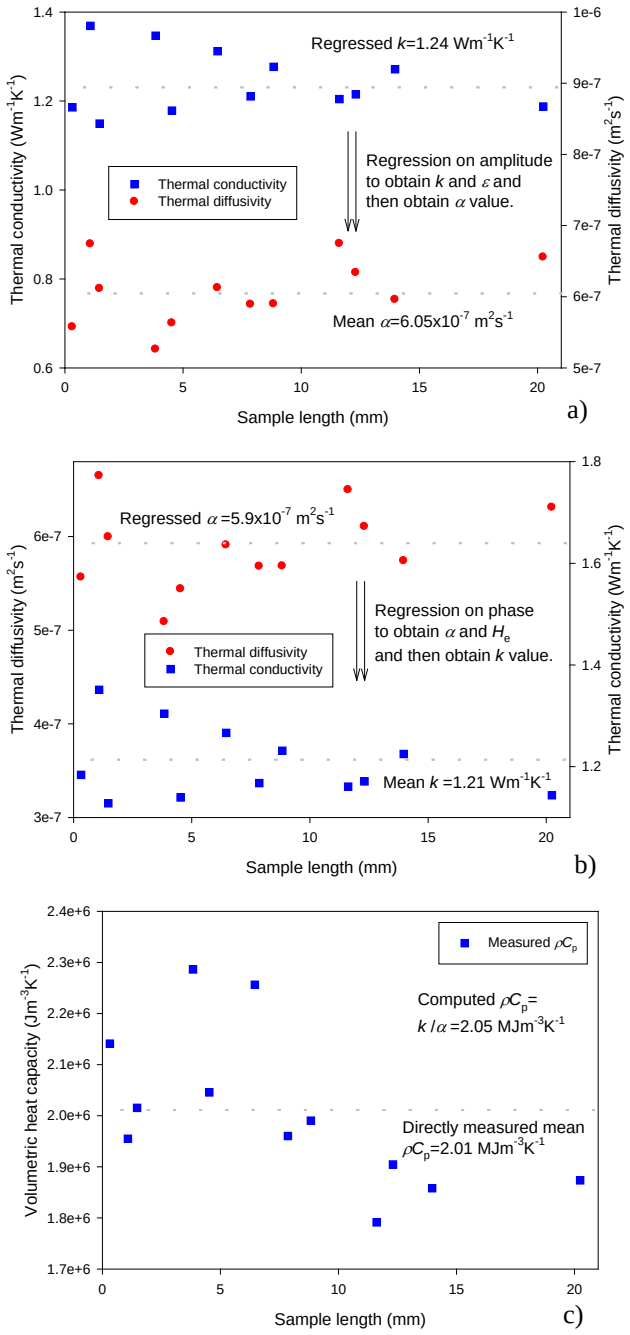

Fig. 4 Thermal conductivity, thermal diffusivity, and volumetric heat capacity of the *dragline silk* by the 3ω technique, a) regression on amplitude to get conductivity and emissivity and then obtain diffusivity, b) regression on phase to get diffusivity and radiation effect and then obtain conductivity, c) directly measured volumetric heat capacity versus computed from k/α, showing good agreement.

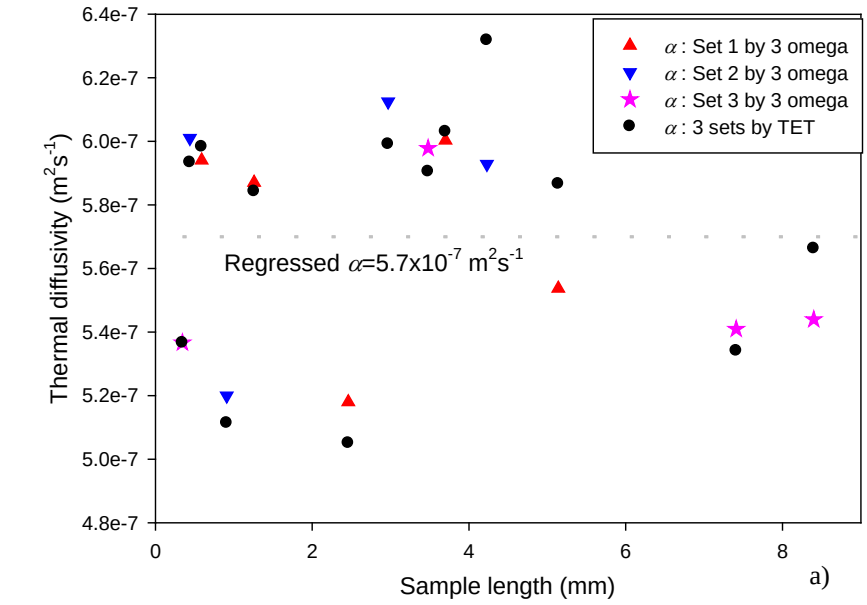

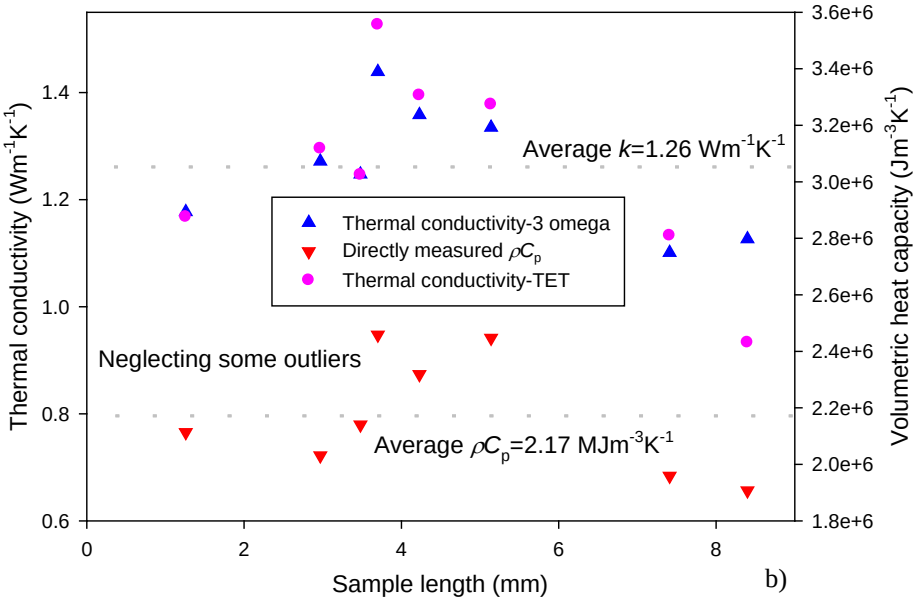

Fig. 5 Thermal conductivity, thermal diffusivity and volumetric heat capacity of the *minor ampullate* silk by the two techniques, a) regression on phase to get diffusivity and radiation effect, b) thermal conductivity by incorporating radiation influence as well as directly measured heat capacity.

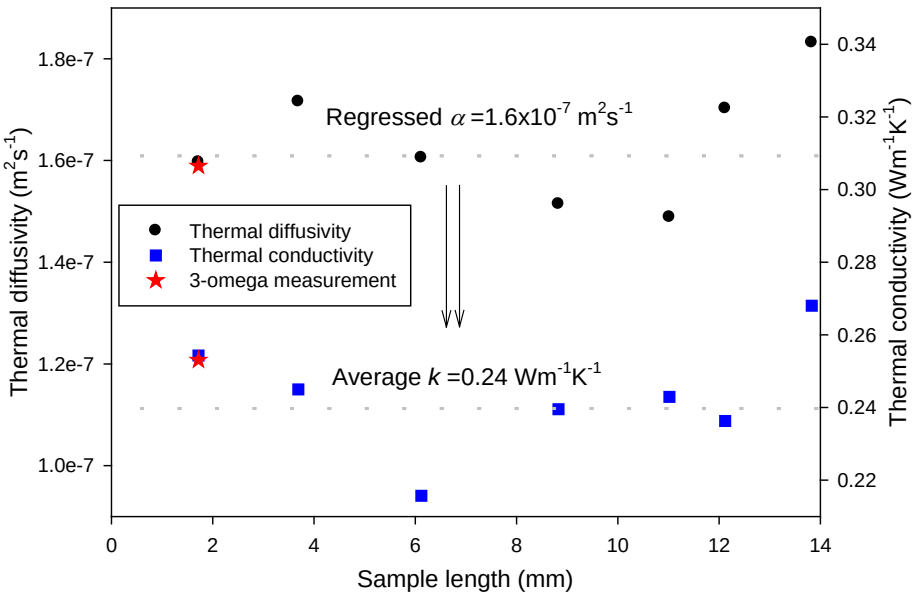

Fig. 6 Thermal property of the as-spun *synthetic silk* by the TET using the (α, $H_e \rightarrow k$) method. Additionally, short fiber 3ω results are shown that have good agreement with the TET results.